Individual Boron Nanowire Has Ultra-High Specific Young's Modulus and Fracture Strength As Revealed by *in Situ* Transmission Electron Microscopy

Fei Liu,[†,∥,*] Dai-Ming Tang,[§,∥] Haibo Gan,[†] Xiaoshu Mo,[†] Jun Chen,[†] Shaozhi Deng,[†] Ningsheng Xu,[†] Yoshio Bando,[‡] and Dmitri Golberg[⊥,*]

[†]State Key Laboratory of Optoelectronic Materials and Technologies, Guangdong ProvinceKey Laboratory of Display Material and Technology, and School of Physics and Engineering, SunYat-sen University, Guangzhou 510275,PR China, [‡]Inorganic Nanostructured Materials Group, International Center for Materials Nanoarchirectonics (MANA), National Institute for Materials Science (NIMS), Namiki 1-1, Tsukuba, Ibaraki 305-0044, Japan, [§]InternationalCenter for Young Scientists (ICYS), National Institute for Materials Science, Namiki 1-1, Tsukuba, Ibaraki 305-0044, Japan, and [⊥]Nanotube Group, International Center for Materials Nanoarchirectonics (MANA), National Institute for Materials Science(NIMS), Namiki 1-1, Tsukuba, Ibaraki 305-0044, Japan. [∥]These authors contributed equally to this work.

ABSTRACT Boron nanowires (BNWs) may have potential applications as reinforcing materials because B fibers are widely known for their excellent mechanical performance. However until now, there have been only few reports on the mechanical properties of individual BNW, and *in situ* transmission electron microscopy (TEM) investigations shining a light on their fracture mechanism have not been performed. In this paper, we applied *in situ* high-resolution TEM (HRTEM) technique to study the mechanical properties of individual BNWs using three loading schemes. The mean fracture strength and the maximum strain of individual BNWs were measured to be 10.4 GPa and 4.1%, respectively, during the tensile tests. And the averaged Young's modulus was calculated to be 308.2 GPa under tensile and compression tests. Bending experiments for the first time performed on individual BNWs revealed that their maximum bending strain could reach 9.9% and their ultimate bending stress arrived at 36.2 GPa. These figures are much higher than those of Si and ZnO nanowires known for their high bending strength. Moreover, the BNWs exhibited very high specific fracture strength (3.9 (GPa · cm^3)/g) and specific elastic modulus (130.6 (GPa · cm^3)/g), which are several dozens of times larger compared to many nanostructures known for their superb mechanical behaviors. At last, the effect of surface oxide layer on the Young's modulus, fracture strength and maximum bending strength of individual BNWs was elucidated to extract their intrinsic mechanical parameters using calculated corrections. All experimental results suggest that the present BNW are a bright promise as lightweight reinforcing fillers.

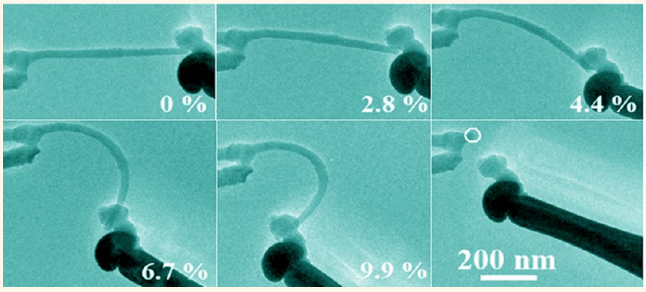

KEYWORDS: boron nanowire (BNW) · *in situ* microscopy · mechanical properties · tensile · compression · bending

Boron nanowires (BNWs) have aroused much attention in the past years because they not only possess low density, high elastic modulus, and high melting-point similar to bulk B materials, but also have a large aspect ratio and high specific surface area.[1−3] With the realization of large-scale synthesis of BNWs,[4−9] they are now considered to be applied as lightweight body armors, micro/nanoelectromechanical systems (MEMS/NEMS) and cantilever-based nanosensors.[10−15] The mechanical properties of BNWs may have a large difference from those of bulk B counter parts because of profound size effects and surface defects, as was referred in other nanostructure systems by severalgroups.[16−26] Although many researches have been focused on the fabrication methods of BNWs,[4−9] up to date, only two papers have been concentrated on the BNW's elastic behaviors.[10,13] Especially, direct *in situ* TEM measurement techniques have not been applied to investigate individual BNW's mechanical performance. Thus, the research on individual BNW's mechanical properties has been lingering far behind of that for many other popular nanostructures, like C nanotubes, ZnO and Si nanowires, *etc.*

* Address correspondence to liufei@mail.sysu.edu.cn, GOLBERG.Dmitri@nims.go.jp.

Received for review August 18, 2013 and accepted October 5, 2013.

Published online October 05, 2013
10.1021/nn404316a

In the previous two studies of BNWs, a mechanical resonance method and an AFM-based technique were, respectively, used to investigate the Young's modulus and fracture strength of individual BNWs.[10,13] In comparison with these two methods, the presently proposed *in situ* TEM technique has two clear advantages, which can be depicted as follows. One is that detailed structure information in regards of individual BNWs at an applied load, including their crystalline structures, fracture planes, defects' distribution, possible amorphous transition, and so on, can be accurately acquired under the tests due to ultimately high spatial resolution peculiar to TEM. The other is that the bending tests may be performed on single BNWs for the first time, which are vital to determine the maximum bending strains and stresses, and the fracture mechanism. Therefore, herein, the tensile, compression and bending experiments have separately been carried out on individual BNWs using *in situ* TEM loadings. In addition, all necessary corrections have been made to eliminate the effect of the surface oxide on the BNWs' mechanical properties and to obtain the BNW's intrinsic mechanical parameters.

RESULTS AND DISCUSSION

Large-scale BNW arrays have successfully been fabricated on a Si(001) substrate by optimizing the experimental parameters, as shown in Figure 1A. Figure 1B gives the side view of the as-grown BNWs. BNWs have a mean length of 6 μm and their diameter ranges from 20 to 40 nm. They have a smooth surface and uniform morphology. Typical TEM and HRTEM images of the BNW are, respectively, provided in Figure 1, panels C and D, to confirm their crystalline structure. The lattice fringe separation between the adjacent growth planes is about 5.1 Å and the corresponding diffraction spots are very clear, which reveals that the nanowire is a single crystalline BNW having an α-tetragonal lattice and the growth direction along the [001] orientation. Moreover, it is noted that an amorphous boron oxide layer with a thickness of about 1−2 nm exists on the BNW. This may affect the elastic behavior of the BNW during the following *in situ* measurements.

First, the tensile tests were performed on three individual BNWs. The corresponding schematic illustration is shown in Figure 2A. From the diagram, one can see that a single BNW is tightly clamped between the AFM cantilever and the tungsten tip utilizing an electron-beam-induced carbon deposition (EBID) technique.[11,21,22,27,28] This technique can ensure that the contact sites can bear high applied force and the structure would not slip out of the clamps until it breaks. In mechanical tests, the cantilever's displacement and the nanowire's elongation or deflection can be accurately measured under HRTEM. Moreover, the applied load is continuously imposed on the BNW by the piezo-driven W tip to generate deformation.

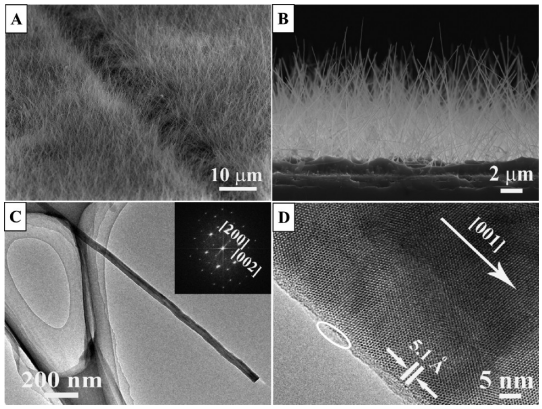

Figure 1. (A) SEM images of large-scale-fabricated BNWs.(B) Side view of the as-grown BNW arrays. (C and D) Typical TEM and HRTEM images of the BNWs. The inset is their corresponding SAED pattern; the white circle refers to the amorphous oxide layer covered on the surface of the BNW.

The whole measurement process can be *in situ* recorded in a real time.

Before the mechanical tests were performed on the individual BNWs, the cantilever used in the measurement had been calibrated to eliminate the possible experimental errors and its nominal spring constant was determined to be 6.9 N/m by a procedure commonly depicted in our previous works.[21,22,27] A series of TEM images during the tensile test are shown in Figure 2B. From these images, it can be seen that the BNW's length gradually becomes larger with an increase of the applied load until abrupt fracture. The white arrow refers to the broken site of the nanowire. This is located at some distance from the clamped sites. It suggests that the fracture under tension truly reflects the intrinsic mechanical behaviors of the BNW rather than the mechanical properties of the clamped sites.

An HRTEM image of the BNW's fracture surface is depicted in Figure 2C. The fracture surface is flat and perpendicular to the growth direction of the nanowire. It is also seen that the broken BNW is still a single crystal and not any crystal−amorphous transition has been taken place within the fractured region. Moreover, no obvious plastic deformation can be traced during the whole tensile test and the breakage of the nanowire occurs suddenly, so the fracture mode is brittle. The stress−strain ($\sigma-\varepsilon$) curves of three individual BNWs are demonstrated in Figure 2D. The stress σ can be calculated by a simple equation of $\sigma = (F/S)$, where F is the applied force, $S = \pi r^2$ is the nanowire's cross-sectional area, and r is the radius of the BNW. The strain ε can be determined using the following equation:

$$\varepsilon = \frac{l - l_0}{l_0} = \frac{\Delta l}{l_0} \qquad (1)$$

where l is the length of the nanowire after elongation, l_0 is the original length of the nanowire before tension, and Δl is the displacement of the nanowire along the applied force direction. The values of $l$and l_0 can be

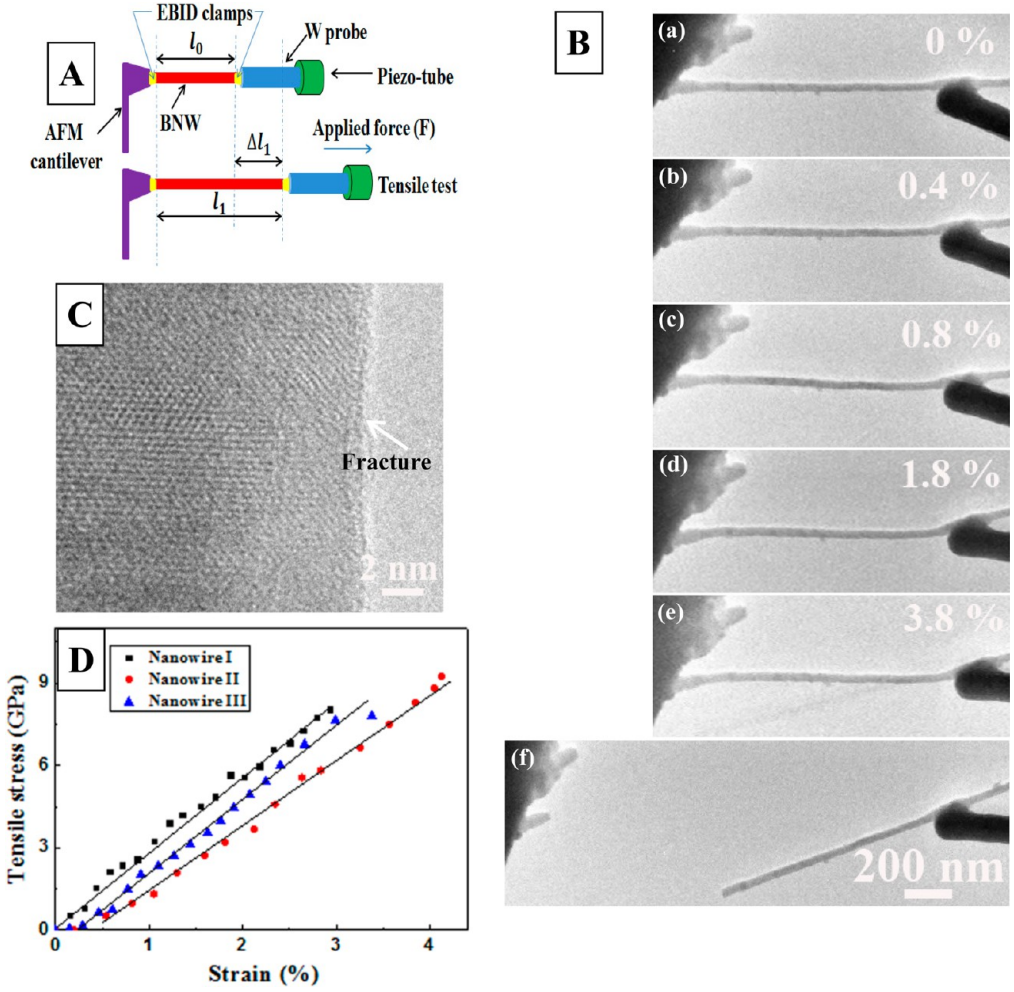

Figure 2. (A) Schematic illustration of the *in situ* tensile measurement. (B) *In situ* TEM images of the tensile experiment at different deformation stages. (C)The HRTEM images of the fracture structure of an individual BNW. The fracture surface is referred by the white arrow. (D) The stress−strain curves of three individual BNWs during the tensile tests.

accurately obtained by measuring them on the HRTEM images *in situ* taken at different applied loads. It is clearly seen that the $\sigma-\varepsilon$ curves of all three BNWs are almost linear, which corresponds to the elastic deformation. Therefore, on the basis of the Hooke's law ($E = (\sigma/\varepsilon)$), the Young's modulus E of the BNWs can be deduced by calculation of the curves' tangents. The tensile stresses of all three BNWs suddenly dropped to zero at failures, which coincides with the observed sudden breaking phenomena caught on *in situ* videos (Supporting Information Video I) showing perfect temporal resolution of the force recording method. Moreover, the fracture strength σ_b of the BNWs ranges from 8.0 to 9.5 GPa and their Young's modulus varies from 238.8 to 270.4 GPa, if one neglects the effect of the surface oxide layers.

A typical thickness of surface amorphous B_2O_3 layer is from 1 to 2 nm and the Young's modulus of bulk B_2O_3 is nearly 10 times lower than that of bulk boron; still the effect of a surface B_2O_3 layer needs to be considered to get refined elastic parameters. According to the classical mechanics theory of compound materials,[29−31] the total force F on individual nanowire's cross-sectional area should be distributed within the two sections, which can be described as

$$F = \sigma S = F_B + F_{oxide} = \sigma_B S_B + \sigma_{oxide} S_{oxide} \quad (2)$$

where F_B and σ_B are, respectively, the force and the stress applied on the core BNW area, F_{oxide} and σ_{oxide} are, respectively, the force and the stress applied on the amorphous oxide shell's area, S_B and S_{oxide} are, respectively, the core BNW's area and the surface oxide shell's area, and σ and S are the above-mentioned stress and the area of the nanowire before correction. If r_{out} and r_{in} correspondingly refer to the outer and inner radius of the nanowire, S_B should be written as $S_B = \pi r_{in}^2$, and S_{oxide} should be expressed as $S_{oxide} = \pi(r_{out}^2 - r_{in}^2)$. On the basis of the Hooke's law, the expressions of $\sigma_B = \varepsilon_B E_B$ and $\sigma_{oxide} = \varepsilon_{oxide} E_{oxide}$ can be easily obtained. Substituting the expression for the area and stress into the eq 2, the total force F can be derived as

$$F = \varepsilon E \pi r_{out}^2 = \varepsilon_B E_B S_B + \varepsilon_{oxide} E_{oxide} S_{oxide}$$
$$= \varepsilon\pi[E_B r_{in}^2 + E_{oxide}(r_{out}^2 - r_{in}^2)] \quad (3)$$

TABLE 1. Summary of Mechanical Properties of Individual BNWs

sample	radius (nm)	maximum strain (%)	Young's modulus (GPa)	corrected Young's modulus (GPa)	fracture strength (GPa)	corrected fracture strength (GPa)	maximum bending strain (%)	maximum bending stress (GPa)	corrected maximum bending force (GPa)	broken mode
BNW (tensile)	19.8	3.5	287.8	308.2	8.6	9.3	/	/	/	brittle
BNW (compression)	18.8	2.4	298.4	322.4	/	/	/	/	/	/
BNW V (bending)	14.95	9.9	306.1	367.5	/	/	9.86	30.2	36.2	brittle
BNW (ref 10)	40−50	/	150−280	/	/	/	/	/	/	/
BNW (ref 13)	20−25	1.0−3.0	250−350	270−390	2.2−8.2	2.4−9.2	/	/	/	brittle

where ε stands for the common deformation of the nanowire at the applied force because the displacement ε_B of the core BNW and the displacement ε_{oxide} of the surface oxide shell are the same in the test. Then, the corrected E_B should be expressed as

$$E_B = E\frac{r_{out}^2}{r_{in}^2} - E_{oxide}\left(\frac{r_{out}^2}{r_{in}^2} - 1\right) \quad (4)$$

where E is the uncorrected Young's modulus of the nanowire before the effect of the oxide shell is taken into account. The corrected fracture strength σ_{Boron} can be deduced by eq 4 and its expression is as below:

$$\begin{aligned}\sigma_{Boron} &= \varepsilon_{max}E_B \\ &= \varepsilon_{max}\left[E\frac{r_{out}^2}{r_{in}^2} - E_{oxide}\left(\frac{r_{out}^2}{r_{in}^2} - 1\right)\right] \\ &= \sigma_b\frac{r_{out}^2}{r_{in}^2} - \varepsilon_{max}E_{oxide}\left(\frac{r_{out}^2}{r_{in}^2} - 1\right) \quad (5)\end{aligned}$$

, where ε_{max} is the critical deformation of the nanowire before the fracture occurs and σ_b is the uncorrected fracture strength. Because the outer and inner radii of the nanowire can be easily measured under HRTEM imaging, and the elastic modulus of surface B_2O_3 layer is assumed to be the same with bulk B_2O_3 (16 GPa),[13,32,33] the corrected intrinsic Young's modulus and fracture strength of individual BNW can now be ascertained. The mean experimental error coming from the oxide shell is calculated to be about 6.8% for the elastic modulus, and 7.5% for the fracture strength of individual BNW. To further understand the effect of surface oxide, the comparative individual BNW's elastic properties obtained in different works are listed in Table 1. In comparison with Li *et al.*'s work,[10] the Young's modulus and fracture strength of individual BNW in our work are a little larger because these mechanical parameters have been corrected in our calculations by considering the effect of surface oxide layer. It is found in Table 1 that the mechanical parameters of individual BNWs in our work are close to the tensile results from Ruoff's group.[13] The difference is that we *in situ* measured the surface B_2O_3 shell's thickness of the nanowire under tensile measurements rather than adopting its mean thickness.[13] Moreover, it can also be found that the maximum strain of individual BNW can reach 3.0−4.5% in our work. These values are larger than those for individual BNWs studied by other groups. The latter phenomenon may be attributed to perfect crystallinity and low defect density of BNWs fabricated and measured by us.

Boron is a low-density and high melting-point material, which makes its corresponding nanostructure attractive for applications as reinforcing material. To value the BNW's mechanical behaviors, we compare them with different nanomaterials known for their good elastic properties (summarized in Table S1). It is known that BNWs have a much lower density than that of most of the commonly used nanomaterials, except CNTs and, barely, Si nanowires.[12,18,19,21,34−37] Thus, they have a very high specific fracture strength (3.9 (GPa·cm^3)/g) and specific elastic modulus (130.6 (GPa·cm^3)/g), which are nearly 4−50 times larger than those for ZnO, GaN, InN, W, and Au nanowires.[12,20,38−47] Generally, specific elastic modulus and specific fracture strength are, respectively, defined as the ratio of the elastic modulus and the fracture strength to the material's mass density. These parameters are crucial for various applications, such as airplane wings, bridges, masts and bicycle frames. High specific elastic modulus and fracture strength performance of individual BNWs suggest that they have solid advantages over many nanomaterials in lightweight material reinforcement applications.

Compression tests were also performed on individual BNWs to further comprehend their axial elastic properties. Figure 3A is the scheme of an individual BNW under compression measurement. The consecutive TEM images of individual BNWs at different stages of compression are shown in Figure 3B. One can see that the compression of the BNW is carried out along the horizontal direction paralleling to the nanowire during the whole loading experiment, as referred by the red line in Figure 3B. And it is also seen that the BNW can recover its original shape without any cracks or deformation once the applied force is released. The corresponding compressive force-strain curve is given

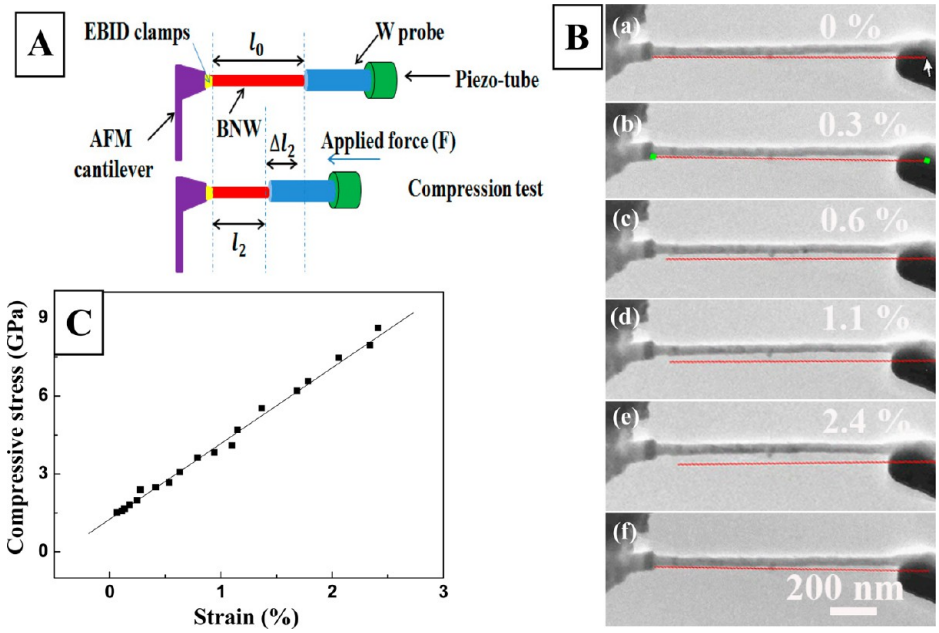

Figure 3. (A) Schematics of individual BNW under compression. (B) Compression process of individual BNW recorded by HRTEM. (C) Typical stress−strain relationship of an individual BNW under compression.

in Figure 3C, in which one can find that the relationship between the stress and the strain keeps linear. It is noted that, if the buckling effect would exist under the compression test, the *F*−*d* curve must exhibit a generally nonlinear behavior as based on the classical mechanics theories and experimental studies.[14,22,30,31] There is not any deviation from the linearity found in our compression measurement, which further excludes the existence of the buckling effect and ensures the accuracy of the present compression data. The maximum strain is 2.4% when the applied stress reaches 8.6 GPa, and the uncorrected Young's modulus of individual BNW is 298.4 GPa. On the basis of the same calculation method, as utilized for tensile measurements, the corrected Young's modulus of a single BNW is computed to be 322.4 GPa after eliminating the effect of the surface oxide layer. So we come to a conclusion that BNWs deformation obeys the Hooke's law and their axial deformation is truly elastic.

Finally, *in situ* bending measurements were carried out to further assess the mechanical performance of individual BNW. The corresponding schematic diagram showing the bending measurement process is provided in Figure 4A. It is found in Figure 4A that the orientation of the applied force is different for the bending tests and the axial tests. The applied load is vertical to the nanowire in the bending test, whereas the applied load is parallel to the nanowire in the tensile and compressive tests. Figure 4B depicts the snapshots of the nanowire during bending, as recorded in sequence under HRTEM. From Figure 4B, it is found that the BNW is undergoing different bending states as the function of the applied force perpendicular to the BNW axis. The nanowire changed from one straight rod to a curved hook, and, at last, was violently damaged from its central region. Using the schematic diagram and the experimental data, we obtained the mechanical parameters of the nanowire under bending. Before the BNW's breakage is initiated, the maximum bending angle between the nanowire and its curvature center reaches 129.6° when the curvature radius arrives at 151.6 nm, which implies that the BNW can withstand very large bending deformation. It is evident in Figure 4C that the fracture surface of the nanowire in bending test is flat and smooth, and is strictly vertical to the growth axis of the nanowire. Moreover, the BNW's diameter at the fracture position is almost the same as in other regions along the nanowire, and the BNW's fracture suddenly emerges when the applied load has reached a critical level. Representative force−nanowire deflection (*F*−*d*) curve of a single BNW is given in Figure 4C. The applied force (vertical to the nanowire's axis) is found to have a linear relationship with the deflection of the structure along the load direction, which implies that BNW's bending should conform to the elastic theory. Also, the force is observed to be abruptly disappeared at a critical deflection in Figure 4D, which corresponds to fracture in the bending test. This mechanical data is in good agreement with the observed results in Figure 4B. This reveals that the fracture of the BNW in bending test is also brittle. The detailed mechanical parameters of individual BNW under bending can be found in Table 1. The maximum bending strain $\varepsilon_{bending}$ of a single BNW arrives at 9.9%. Herein, the expression for the bending strain $\varepsilon_{bending}$ is different with the

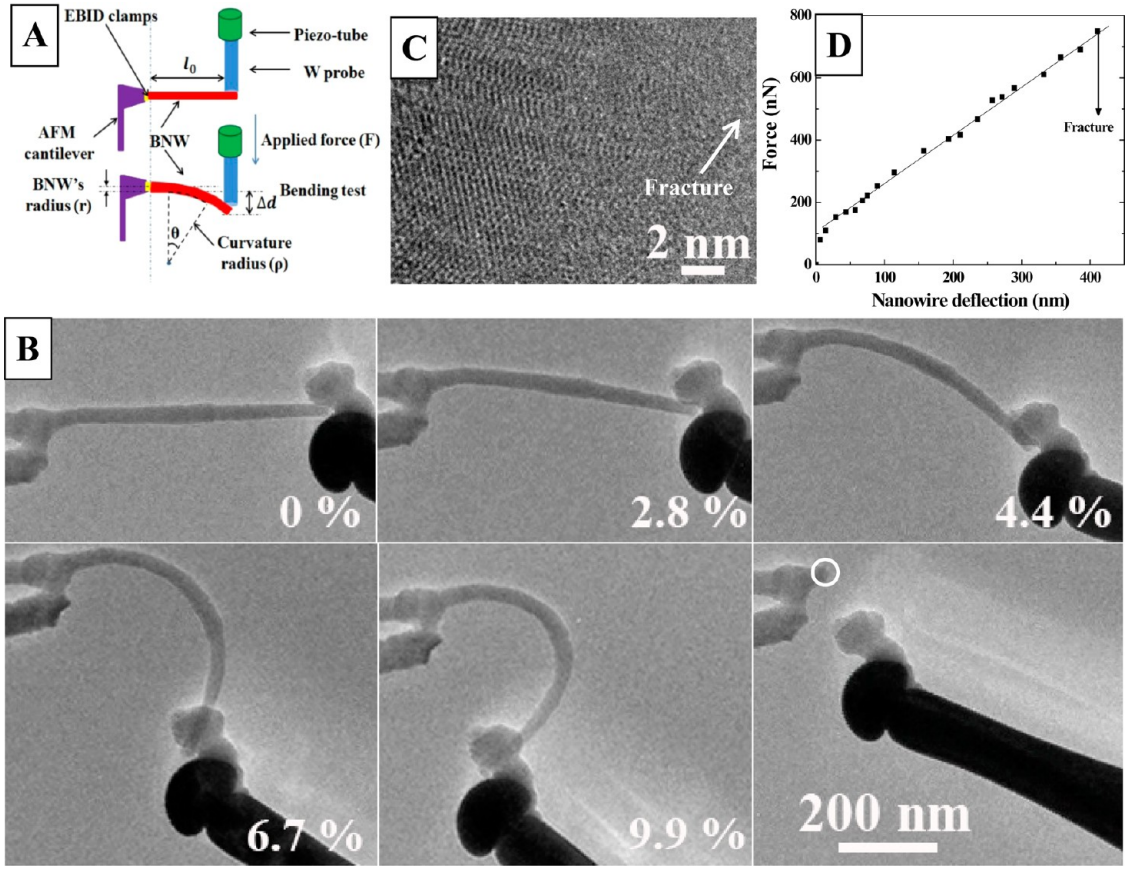

Figure 4. (A) Schematic diagram showing the *in situ* bending measurement setup. (B) Consecutive HRTEM images of an individual BNW during different bending stages. (C) The HRTEM image reveals the surface structure of the BNW after fracture. (D) Typical force-deflection distance curve of the individual BNW in the bending experiment.

strain of the nanowire under elongation, and is given as follows:

$$\varepsilon_{\text{bending}} = \left(\frac{r}{\rho + r}\right) \times 100\% \tag{6}$$

where r is the radius of the BNW and ρ is the curvature radius of the inner edge of the bending BNW, as illustrated in Figure 4A. According to the classical elastic theory,[29−31] the vertical deflection Δd of the BNW can be expressed as

$$\Delta d = \frac{Fl_0^3}{3EI} \tag{7}$$

where F is the vertical applied force, E is the Young's modulus of the BNW, l_0 is the original length of the nanowire before bending, and $I = (1/4)\pi r^4$ is the moment of inertia of the rod-like nanowire. Substituting the expression of I into eq 6, then we obtain

$$\Delta d = \frac{4Fl_0^3}{3E\pi r^4} \tag{8}$$

Then, according to the Hooke's law, the elastic mechanical equation can be written as

$$F = k\Delta d = \frac{3E\pi r^4}{4l_0^3}\Delta d \Rightarrow E = \frac{4l_0^3 k}{3\pi r^4} \tag{9}$$

where the elastic constant k of the BNW is equal to the slope of $F-d$ curve. On the basis of the bending theory of the beam,[29−31] the maximum bending stress σ_B of the nanowire can be described as

$$\sigma_B = \frac{rE}{\rho_{\text{critical}}} \tag{10}$$

where ρ_{critical} is the critical curvature radius of the BNW before fracture. Here, the maximum bending stress is defined as the maximum stress that individual nanowire can bear before the fracture occurs. Therefore, through the aforementioned equations, the maximum bending stress and the Young's modulus of the nanowire can be, respectively, worked out to be 30.2 and 306.1 GPa.

To get rid of the effect of amorphous B_2O_3 layer and obtain the pristine bending properties of the BNW, further corrections were carried out as follows. On the basis of the mechanics theory of the composite materials,[29−31] the relationship between the bending moment M and the curvature radius ρ of the bending nanowire can be expressed as

$$\frac{1}{\rho} = \frac{M}{IE} \Rightarrow M = \frac{EI}{\rho} \tag{11}$$

where E and I are, respectively, the Young's modulus and the moment of inertia of individual BNW. Taking

the existence of the surface oxide shell into account, the total bending moment M is composed of two sections, which are the bending moment M_{oxide} of the surface oxide shell and the bending moment M_B of the core BNW. The curvature radius of the core BNW is the same as that of the oxide shell in the bending process, so the equation of M can be written as

$$M = \frac{EI}{\rho} = M_B + M_{oxide} = \frac{E_B I_B}{\rho} + \frac{E_{oxide} I_{oxide}}{\rho} \quad (12)$$

where E, equal to the slope of $F-d$ curve, is the uncorrected modulus of the BNW, I is the total moment of inertia of the composite nanomaterial, E_B and E_{oxide}, respectively, represent the Young's modulus of the core BNW and the surface oxide shell, and I_B and I_{oxide} correspond to their moment of inertia. Because cross section of BNW is circular, the expressions of the total moments of inertia I and I_{oxide} become

$$I = \frac{1}{4}\pi r_{out}^4,\ I_{oxide} = I - I_B = \frac{1}{4}\pi r_{out}^4 - \frac{1}{4}\pi r_{in}^4 \quad (13)$$

where r_{out} and r_{in} refer to the outer and inner radii of the BNW, respectively. Thus, by substituting eq 13 in eq 12, we find

$$EI = E\frac{1}{4}\pi r_{out}^4 = E_B\frac{1}{4}\pi r_{in}^4 + E_{oxide}\left(\frac{1}{4}\pi r_{out}^4 - \frac{1}{4}\pi r_{in}^4\right) \quad (14)$$

Dividing both parts of eq 14, it becomes

$$E = E_B\left(\frac{r_{in}}{r_{out}}\right)^4 + E_{out}\left[1 - \left(\frac{r_{in}}{r_{out}}\right)^4\right] \quad (15)$$

Then, substituting the corrected E_B instead of E in eq 10, the corrected maximum bending stress is calculated. Because the thickness of the amorphous B_2O_3 shell is 1.4 nm based on the HRTEM observations, the corrected Young's modulus and maximum bending stress of the BNW under bending are obtained as 367.5 and 36.2 GPa, respectively. The maximum bending stress of a single BNW is nearly $^1/_{10}$ of its Young's modulus, which is in good accordance with the ideal proportions of a material in elastic theory.[48,49] It further proves that the mechanical behavior of the bent BNW is elastic up to fracture point. Moreover, it is clear that the averaged maximum bending stress (36.2 GPa) of individual BNWs is much higher than that of ZnO nanowires (4−10 GPa) and Si nanowires (5−18 GPa). This suggests that present BNWs have a strong endurance to large bending stress. Therefore, merging elongation, compression, and bending data on individual BNWs, it can be concluded that they represent ideal lightweight reinforcing materials.

CONCLUSIONS

In situ HRTEM technique is applied to accurately measure the mechanical properties of individual BNWs. With the use of the classical mechanics equations and elastic theory, the intrinsic mechanical parameters of individual BNWs are obtained while eliminating the effects of the surface oxide shell. The mean Young's modulus and averaged fracture strength are, respectively, determined to be 308.2 and 9.3 GPa. And their corresponding specific Young's modulus and fracture strength are found to be 130.6 and 3.9 (GPa·cm^3)/g, which are far higher than for many nanomaterials known for their good elastic behaviors. Moreover, the maximum bending stress of individual BNWs, for the first time derived in the present work, can reach 36.2 GPa when their bending strain arrives at 9.9%. All present findings suggest that BNWs should have a promising future in lightweight materials' reinforcement and MEMS/NEMS applications.

MATERIALS AND METHODS

Synthesis Method. The growth of BNWs was carried out in a simple CVD system, which had been described in our recent works.[6,50] B_2O_3 powders (99.99%) and B powders (99.99%) (mass ratio is 1:1) were mixed together to be used as source materials. A Ni film is sputtered on the surface of silicon wafer to work as a catalyst. The base pressure of the vacuum chamber was lower than 7 Pa and the carrier gas was a mixed gas of Ar and H_2 (flow rate ratio is 300:200 sccm). After keeping the reaction vessel at 1100 °C for 2−4 h, the furnace was cooled to room temperature in Ar gas and BNWs formed on the surface of the Si substrate.

Morphology and Structure Characterization. A field-emission type scanning electron microscope (XL-SFEG SEM, FEI Corp.) and transmission electron microscope (JEM-3000F, JEOL Corp.) were used to investigate the morphology and crystalline structures of the as-prepared BNWs, respectively.

***In Situ* Mechanical Property Measurement.** *In situ* measurements of the mechanical properties of individual BNWs were performed in a field emission high-resolution transmission electron microscope (JEM-3100FEF, JEOL Corp.; spatial resolution is 0.17 nm) equipped with a "Nanofactory Instrument" AFM-TEM piezo-driven holder, as described in our recent research.[22] First, the BNWs were dispersed in ethanol solutions after they had been peeled off from a Si wafer. Subsequently, both ends of the BNWs were, respectively, fixed on the W tip and the AFM cantilever (to ensure that tight cohesion will exist in the following measurement) by depositing a layer of carbon film on their contact sites. Finally, three-dimensional manipulations of individual BNWs on W tips can be precisely controlled (step is better than 0.1 nm) by driving of the piezo-motor. The BNWs' performance and experimental data were real-time recorded by a commercial film grabber.

Conflict of Interest: The authors declare no competing financial interest.

Supporting Information Available: More detailed experimental data on the individual BNW, such as the EEL spectrum and the *in situ* measurement videos of individual BNW, as well as the comparative table showing mechanical parameters of individual BNW and other nanostructures. This material is available free of charge *via* the Internet at http://pubs.acs.org.

Acknowledgment. This work was supported by National Key Basic Research Program of China (Grant No. 2010CB327703, 2013CB933601), the National Natural Science Foundation of China (Grant No. 51072237, U1134006), the Fundamental Research Funds for the Central Universities (2009-30000-3161452), the Natural Science foundation of Guangdong Province

(No. S2012010010519), Program for New Century Excellent Talents in University (NCET-12-0573), China Scholarship Council Fund for Young Backbone Teacher, the Science and Technology Department of Guangdong Province, and the Nanotube Unit of the World Premier International Center for Materials Nanoarchitectonics (WPI-MANA) of the National Institute for Materials Sciences, Namiki 1-1, Tsukuba, Ibaraki, Japan 305-0044.

REFERENCES AND NOTES

1. *Boron and Refractory Borides*; Matkovich, V. I., Ed.; Springer: New York, 1977; pp 15−35.
2. *Boron, Metallo-Boron Compounds and Boranes*; Adams, R. M., Ed.; Wiley Interscience: New York, 1964; pp 170−180.
3. *The Structure of the Elements*; Konohue, J., Ed.; Krieger: Malabar, 1982; pp 81−95.
4. Tian, J. F.; Hui, C.; Bao, L. H.; Li, C.; Tian, Y.; Ding, H.; Shen, C. M.; Gao, H. J. Patterned Boron Nanowires and Field Emission Properties. *Appl. Phys. Lett.* **2009**, *94*, 083101.
5. Wang, X. J.; Tian, J. F.; Yang, T. Z.; Bao, L. H.; Hui, C.; Liu, F.; Shen, C. M.; Gu, C. Z.; Xu, N. S.; Gao, H. J. Single Crystalline Boron Nanocones: Electric Transport and Field Emission Properties. *Adv. Mater.* **2007**, *19*, 4480–4485.
6. Liu, F.; Tian, J. F.; Bao, L. H.; Yang, T. Z.; Shen, C. M.; Lai, X. Y.; Xiao, Z. M.; Xie, W. G.; Xu, N. S.; Gao, H. J.; et al. Fabrication of Vertically Aligned Single Crystalline Boron Nanowire Arrays and Investigation on Their Field Emission Behaviors. *Adv. Mater.* **2008**, *20*, 2609–2615.
7. Wu, Y. Y.; Messer, B.; Yang, P. D. Superconducting MgB_2 Nanowires. *Adv. Mater.* **2001**, *13*, 1487–1489.
8. Cao, L. M.; Zhang, Z.; Sun, L. L.; Gao, C. X.; He, M.; Wang, Y. Q.; Li, Y. C.; Zhang, X. Y.; Li, G.; Wang, W. K.; *et al.* Well Aligned Boron Nanowire Arrays. *Adv. Mater.* **2001**, *13*, 1701–1704.
9. Otten, C. J.; Lourie, O. R.; Yu, M. F.; Cowley, J. M.; Ruoff, R. S.; Buhro, W. E. Crystalline Boron Nanowires. *J. Am. Chem. Soc.* **2002**, *124*, 4564–4565.
10. Lin, C. H.; Ni, H.; Wang, X. N.; Chang, M.; Chao, Y. J.; Deka, J. R.; Li, X. D. *In Situ* Nanomechanical Characterization of Single-Crystalline Boron Nanowires by Buckling. *Small* **2010**, *6*, 927–931.
11. Tao, X. Y.; Dong, L. X.; Wang, X. N.; Zhang, W. K.; Nelson, B. J.; Li, X. D. B_4C-Nanowires/Carbon-Microfiber Hybrid Structures and Composites from Cotton T-shirts. *Adv. Mater.* **2010**, *22*, 2055–2059.
12. Rolhig, C. C.; Niebelschutz, M.; Brueckner, K.; Tonisch, K.; Ambacher, O.; Cinalla, V. Elastic Properties of Nanowires. *Phys. Status Solidi B* **2010**, *247*, 2557–2570.
13. Ding, W. Q.; Calabri, L.; Chen, X. Q.; K. Kohlhaas, M.; Ruoff, R. S. Mechanics of Crystalline Boron Nanowires. *Compos. Sci. Technol.* **2006**, *66*, 1112–1124.
14. Hsin, C. L.; Mai, W. J.; Gu, Y. D.; Gao, Y. F.; Huang, C. T.; Chen, L. J.; Wang, Z. L. Elastic Properties and Buckling of Silicon Nanowires. *Adv. Mater.* **2008**, *20*, 3919–3923.
15. Yang, S. Z.; Wang, L.; Tian, X.; Xu, Z.; Bai, X. D.; Wang, E. G. The PiezotronicEffect of Zinc Oxide Nanowires Studied by *in Situ* TEM. *Adv. Mater.* **2012**, *24*, 4676–4682.
16. Bai, X. D.; Gao, P. X.; Wang, Z. L.; Wang, E. G. Dual-Mode Mechanical Resonance of Individual ZnO Nanobelts. *Appl. Phys. Lett.* **2003**, *82*, 4806–4808.
17. Wang, L. H.; Zhang, Z.; Han, X. D. *In Situ* Experimental Mechanics of Nanomaterials at the Atomic Scale. *NPG Asia Mater.* **2013**, *5*, e40.
18. Gordon, M. J.; Baron, T.; Dhalluin, F.; Gentile, P. Ferret, P. Size Effects in Mechanical Deformation and Fracture of Cantilevered Silicon Nanowires. *Nano Lett.* **2009**, *9*, 525–529.
19. Wang, L. H.; Zheng, K.; Zhang, Z.; Han, X. D. Direct Atomic-Scale Imaging about the Mechanisms of Ultralarge Bent Straining in Si Nanowires. *Nano Lett.* **2011**, *11*, 2382–2385.
20. Lu, Y.; Song, J.; Huang, J. Y.; Lou, J. Fracture of Sub-20 nm Ultrathin Gold Nanowires. *Adv. Funct. Mater.* **2011**, *21*, 3982–3989.
21. Tang, D. M.; Ren, C. L.; Wang, M. S.; Wei, X. L.; Kawamoto, N.; Liang, C.; Bando, Y.; Mitome, M.; Fukata, N.; Golberg, D. Mechanical Properties of Si nanowires as Revealed By *In Situ* Transmission Electron Microscopy and Molecular Dynamics Simulations. *Nano Lett.* **2012**, *12*, 1898–1904.
22. Golberg, D.; Costa, P. M. F. J.; Wang, M. S.; Wei, X. L.; Tang, D. M.; Xu, Z.; Huang, Y. H.; Gautam, U. K.; Liu, B. D.; Zeng, H.; *et al.* Nanomaterial Engineering and Property Studies in a Transmission Electron Microscope. *Adv. Mater.* **2012**, *24*, 177–194.
23. Yue, Y. H.; Liu, P.; Zhang, Z.; Han, X. D.; Ma, E. Approaching Theoretical Elastic Strain Limit in Nano Copper Crystals. *Nano Lett.* **2011**, *11*, 3151–3155.
24. Deng, Q. S.; Cheng, Y. Q.; Yue, Y. H.; Zhang, L.; Zhang, Z.; Han, X. D.; Ma, E. High Elastic Strain Limit and Uniform Elongation of Metallic Glass Nanowires at Room Temperature. *Acta Mater.* **2011**, *59*, 6511–6518.
25. Zheng, K.; Han, X. D.; Wang, L. H.; Zhang, Y. F.; Yue, Y. H.; Qin, Y.; Zhang, X. N.; Zhang, Z. Atomic Mechanisms Governing the Elastic Limit and the Incipient Plasticity of Bending Si Nanowires. *Nano Lett.* **2009**, *9*, 2471–2476.
26. Tian, L.; Cheng, Y. Q.; Shan, Z. W.; Li, J.; Wang, C. C.; Han, X. D.; Sun, J.; Ma, E. Approaching the Ideal Elastic Limit of Metallic Glasses. *Nat. Commun.* **2012**, *3*, No. 609.
27. Wang, M.; Wang, J. Y.; Chen, Q.; Peng, L. M. Fabrication and Electrical and Mechanical Properties of Carbon Nanotube Interconnections. *Adv. Funct. Mater.* **2005**, *15*, 1825–1831.
28. Wei, X. L.; Wang, M. S.; Bando, Y.; Golberg, D. Tensile Tests on Individual Multi-Walled Boron Nitride Nanotubes. *Adv. Mater.* **2010**, *22*, 4895–4899.
29. Timoshenko, S. *Strength of Materials: Part I*; Van Nostrand: New York, 1940; pp 65−84.
30. *Mechanics of Materials*, 6th ed.; Beer, F. P., Johnston, E. R., DeWolf, J. T., Jr., Mazurek, D. F., Eds.; McGraw-Hill: New York, 2012; pp 222−244.
31. *Theory of Mechanics*, 2nd ed.; Landau, L. D., Lifshitz, E. M., Eds.; Pergamon Press: London, 1970; pp 75−89.
32. Tavadze, F. N.; Lominadze, J. V.; Khuvedelidze, A. G.; Tsagareishvili, G. V.; Shorshorov, M. K.; Bulichev, S. I. The Effect of Impurities on the Mechanical Properties of Zone-Melted Boron. *J. Less-Common Met.* **1981**, *82*, 95–99.
33. Ramos, M. A.; Moreno, J. A.; Vieira, S.; Prieto, C.; Fernandez, J. F. Correlation of Elastic, Acoustic and Thermodynamic Properties in B_2O_3 Glasses. *J. Non-Cryst. Solids* **1997**, *221*, 170–180.
34. Stan, G.; Krylyuk, S.; Davydov, A. V.; Levin, I.; Cook, R. F. Ultimate Bending Strength of Si Nanowires. *Nano Lett.* **2012**, *12*, 2599–2604.
35. Yu, M. F.; Lourie, O.; Dyer, M. J.; Moloni, K.; Kelly, T. F.; Ruoff, R. S. Strength and Breaking Mechanism of Multiwalled Carbon Nanotubes Under Tensile Load. *Science* **2000**, *287*, 637–640.
36. Zhang, H.; Tang, T.; Zhu, P. W.; Ma, J.; Qin, L. C. High Tensile Modulus of Carbon Nanotube Nano-Fibers Produced by Dielectrophoresis. *Chem. Phys. Lett.* **2009**, *478*, 230–233.
37. Demczyk, B. G.; Wang, Y. M.; Cumings, J.; Hetman, M.; Han, W.; Zettl, A.; Ritchie, R. O. Direct Mechanical Measurement of the Tensile Strength and Elastic Modulus of Multiwalled Carbon Nanotubes. *Mater. Sci. Eng., A* **2002**, *334*, 173–178.
38. Agrawal, R.; Peng, B.; Espinosa, H. D. Experimental-Computational Investigation of ZnO Nanowires Strength and Fracture. *Nano Lett.* **2009**, *9*, 4177–4183.
39. Xu, F.; Qin, Q. Q.; Mishra, A.; Gu, Y.; Zhu, Y. Mechanical Properties of ZnO Nanowires Under Different Loading Modes. *Nano Res.* **2010**, *3*, 271–280.
40. Chen, C. Q.; Shi, Y.; Zhang, Y. S.; Zhu, J.; Yan, Y. J. Size Dependence of Young's Modulus in ZnO Nanowires. *Phys. Rev. Lett.* **2006**, *96*, No. 075505.
41. Hoffmann, S.; Ostlund, F.; Michler, J.; Fan, H. J.; Zacharias, M.; Christiansen, S. H.; Ballif, C. Fracture Strength and Young's Modulus of ZnO Nanowires. *Nanotechnology* **2007**, *18*, No. 205503.
42. Nam, C. Y.; Jaroenapibal, P.; Tham, D.; Luzzi, D. E.; Evoy, S.; Fischer, J. E. Diameter-Dependent Electromechanical Properties of GaN Nanowires. *Nano Lett.* **2006**, *6*, 153–158.
43. Rolhig, C. C.; Niebelschutz, M.; Cinalla, V.; Cai, Z. H.; Veereddy, D.; Tao, X. Y.; Li, X. D.; Webb, R. A.; Koley, G.

Structural and Elastic Properties of InN Nanowires. *Phys. Status Solidi A* **2012**, *209*, 718–723.
44. Cimalla, V.; Rohlig, C. C.; Peozldt, J.; Niebelschutz, M.; Ambacher, O.; Bruckner, K.; Hein, M.; Weber, J.; Milenkovic, S.; Smith, A. J.; Hassel, A. W. Nanomechanics of Single Crystalline Tungsten Nanowires. *J. Nanomater.* **2008**, *2008*, No. 638947.
45. Pugachevskii, M. A. Determining Elastic Moduli of Tungsten Nanowires. *Tech. Phys. Lett.* **2010**, *36*, 639–641.
46. Wu, B.; Heidelberg, A.; Boland, J. J. Mechanical Properties of Ultrahigh-Strength Gold Nanowires. *Nat. Mater.* **2005**, *4*, 525–529.
47. Marszalek, P. E.; Greenleaf, W. J.; Li, H. B.; Oberhauser, A. F.; Fernandez, J. M. Atomic Force Microscopy Captures Quantized Plastic Deformation in Gold Nanowires. *Proc. Natl. Acad. Sci. U.S.A.* **2000**, *97*, 6282–6286.
48. *Strength and Fracture of Engineering Solids*; Felbeck, D. K., Atkins, A. G., Eds.; Prentice-Hall: Englewood Cliffs, NJ, 1984; pp 393−424.
49. *Strong Solids*, 3rd ed.; Kelly, A., Macmillan, N. H., Eds.; Oxford University: New York, 1986; pp40−69.
50. Liu, F.; Gan, H. B.; Tang, D. M.; Cao, Y. Z.; Mo, X. S.; Chen, J.; Deng, S. Z.; Xu, N. S.; Golberg, D.; Bando, Y. Growth of Large-Scale Boron Nanowire Patterns with Identical Base-Up Mode and *In-Situ* Field Emission Studies of Individual Boron Nanowire. *Small* **2013**, 10.1002/smll.201301948.